Modeling Nonlinear Interference with Sparse Raman-Tilt Equalization

Modeling Nonlinear Interference With Sparse Raman-tilt Equalization

Chiara Lasagni, *Student Member, IEEE,* Paolo Serena, *Member, IEEE,*and Alberto Bononi, *Senior Member, IEEE*

***Abstract*—We investigate the impact of accumulated stimulated Raman scattering (SRS) on the nonlinear interference (NLI) variance due to sparse gain-tilt equalization along the optical link. We propose simple modifications to analytical models available in the literature, such as the Gaussian noise (GN) or the enhanced Gaussian noise (EGN) models, for reliable NLI estimation in the presence of accumulated SRS. We additionally generalize closed-form expressions of the NLI variance in a GN framework to the new scenario. We validate the models through split-step Fourier method simulations showing the importance of including the gain-tilt equalization period in the model to preserve the accuracy. The proposed model is then used to provide insights on the interplay between the NLI and accumulated SRS.**

***Index Terms*—Stimulated Raman scattering (SRS), Dynamic gain equalizer (DGE), Gaussian noise (GN) model, enhanced Gaussian noise (EGN) model.**

I. Introduction

EXPLOITING the bandwidth of the optical fiber is the first choice to increase the capacity of current optical communication systems. In particular, a widespread solution adopted by vendors is the deployment of multi-band C+L systems [1]. Besides the technological problems, one of the main challenges for the system designer is represented by the estimation of the system performance, for which analytical models stand out as the best low-complexity candidates. In fact, accurate split-step Fourier method (SSFM) simulations may become prohibitive due to the computational effort required to simulate the propagation of wavelength division multiplexing (WDM) signals spanning the whole C+L band, or even wider bandwidths, over long-haul links [2].

Perturbative analytical models, such as the Gaussian noise (GN) model [3], are nowadays widely used to estimate the nonlinear interference (NLI) arising along propagation and the corresponding signal-to-noise (SNR) ratio. The GN model represents a simple and fast tool, whose accuracy is further improved by its modulation format-aware version, known as the enhanced Gaussian noise (EGN) [4], [5] or nonlinear interference noise (NLIN) model [6]. Unfortunately, the reliability of these models in ultra-wideband transmissions is undermined by the presence of inter-channel stimulated Raman scattering (SRS).

SRS is a nonlinear process for which higher signal frequencies are depleted while amplifying lower frequencies, yielding a tilted signal power profile [7]. As a side effect, the strength of the nonlinear Kerr effect changes, with an effect increasingly important for increasing bandwidths.

An extension of the GN model to include inter-channel SRS in a multi-span link was proposed in [8]–[10]. In particular, the work in [10] used an analytical expression of the signal power profile in the presence of SRS. This expression is based on the triangular approximation of the Raman gain in the frequency domain [11], [12] and the assumption that all spans are identical, with Raman gain tilt on the signal power perfectly equalized at the end of each span.

The GN model is able to estimate the individual contributions of self-phase modulation (SPM), cross-phase modulation (XPM), four-wave mixing (FWM), cross- and multi-channel interference (XCI, MCI), according to the NLI nomenclature in [2]. Since SPM and XPM are generally dominant in highly-dispersive links, several works concentrated on finding simple expressions for SPM and XPM. Closed-form expressions including SRS in a GN-framework were proposed in [13], [14]. In [14], the authors also introduced the use of fitting parameters to cope with non-uniform power profiles. In [15] a correction term for XPM accounting for the modulation format is presented. To fully include the impact of the modulation format, the EGN model has been extended to account for SRS in [2], [16].

The short computational time of Raman-aware GN models enables addressing complex design problems, such as the optimal signal power allocation at the transmitter side to counteract the SRS effect, as done in [8], [17]. In both works, the authors tackled the problem of optimal power allocation in the presence of uncompensated SRS. These studies were motivated by the fact that in practical systems the dynamic gain equalizers (DGEs) for the compensation of the SRS on the signal power are not placed after each span. For instance, a compensation period value of 4-5 spans can be found in the terrestrial systems literature [1], [8], [9].

In this work, we show that such a sparse DGE positioning has a relevant impact on the system performance, and thus on the models' accuracy. We extend the Raman-aware EGN model of [2], [16] to scenarios where the SRS gain equalization is not performed at every span. The proposed model includes the interaction between nonlinear Kerr effect and accumulated SRS in a modulation format-aware manner, as well as a signal-power pre-emphasis at the transmitter side. Finally, we extend the closed-form expressions of [14] to include such sparse DGE positioning along the link. This work is an extended version of [18] that includes all the needed mathematical derivations.

The authors are with the Department of Ingegneria e Architettura, Università di Parma, Parma 43124, Italy (e-mail: chiara.lasagni@unipr.it, paolo.serena@unipr.it, alberto.bononi@unipr.it).

This work was supported by the Italian PRIN 2017 project Fiber Infrastructure for Research on Space-Division Multiplexed Transmission (FIRST).

The remainder of this paper is organized as follows. In Section II we review NLI models from the literature and we propose a method to account for generic DGE placement in the link. In Section III we propose approximated models which aim at reducing the model complexity, including closed-form expressions for the GN-term based on [14]. Section IV is devoted to numerical results. Finally, in Section V we will draw our conclusions.

II. Nonlinear interference modeling

Under a first-order perturbative approximation [19] of the Manakov equation[1], the received field of a generic optical-link, after removing linear propagation effects, takes the following expression at coordinate z

$$\vec{A}(z,\omega) \approx \vec{A}(0,\omega) + \vec{w}(z,\omega) + \vec{n}(z,\omega) \tag{1}$$

where: $\vec{A}(0,\omega)$ is the transmitted dual-polarization signal field at angular frequency ω, $\vec{w}(z,\omega)$ is the received amplified spontaneous emission (ASE) noise field due to optical amplifiers, while $\vec{n}(z,\omega)$ accounts for the nonlinear interference which, neglecting signal-noise interaction, is:

$$\vec{n}(z,\omega) = -j\frac{8}{9}\gamma \iint_{-\infty}^{\infty} \eta(\omega,\omega_1,\omega_2)\vec{A}^{\dagger}(0,\omega+\omega_1+\omega_2)\times \vec{A}(0,\omega+\omega_2)\vec{A}(0,\omega+\omega_1)\frac{\mathrm{d}\omega_1}{2\pi}\frac{\mathrm{d}\omega_2}{2\pi}. \tag{2}$$

Here γ is the fiber nonlinear coefficient, $\dagger$ represents transpose-conjugate, while $\eta(\omega,\omega_1,\omega_2)$ stands for the so-called fiber kernel (also known as link function) weighting the FWM interaction among signal frequencies. For a dispersion-uncompensated link composed of N identical spans, each of length L, such a fiber kernel can be written as [8]–[10], [13]

$$\eta(\omega,\omega_1,\omega_2) = \sum_{k=1}^{N} e^{j\Delta\beta(k-1)L}\int_0^L e^{j\Delta\beta\zeta}\times \sqrt{\frac{\rho_k(\zeta,\omega+\omega_1+\omega_2)\rho_k(\zeta,\omega+\omega_1)\rho_k(\zeta,\omega+\omega_2)}{\rho_k(\zeta,\omega)}}\mathrm{d}\zeta, \tag{3}$$

where $\rho_k(\zeta,\omega)$ is the frequency-dependent normalized power profile from the transmitter up to the local coordinate ζ within span k. The phase-matching coefficient $\Delta\beta$ is defined as

$$\begin{aligned}\Delta\beta &\triangleq \beta(\omega) - \beta(\omega+\omega_1) - \beta(\omega+\omega_2) + \beta(\omega+\omega_1+\omega_2)\\ &= \omega_1\omega_2\Big[\beta_2 + \frac{1}{2}(2\omega+\omega_1+\omega_2)\beta_3\Big]\end{aligned} \tag{4}$$

where β is the propagation constant, and β_2 and β_3 its second and third-order coefficients evaluated at the reference frequency of the lowpass equivalent spectrum. Such a model includes in the term ρ_k any positioning of the DGE along the link.

In the following, NLI expressions based on different power profiles are presented, starting from a literature review in Sec. II-A and II-B. These expressions serve as a starting point for the computation of the NLI power spectral density [3, Eq. (1)], [4, Eq. (5)-(26)], [5, Tab. 1], and variance [6, Eq. (25)].

[1]The reasons for using the Manakov equation instead of the coupled Nonlinear Shrödinger equation are discussed in e.g. [2, App. A].

A. Absence of SRS

With end-span lumped amplification and without SRS, the signal propagating along the optical link undergoes fiber attenuation and optical amplification. Assuming that each amplifier perfectly recovers the fiber losses, the normalized power profile in Eq. (3) can be written as

$$\rho(\zeta) = e^{-\alpha\zeta} \tag{5}$$

where α is the fiber attenuation, here assumed frequency-independent. The assumption of ideal amplifiers yields a span independent power profile, due to the absence of accumulated losses from the previous spans, which coincides with the power profile of a single-span link. With the substitution of Eq. (5) in Eq. (3) the link kernel writes in the compact form

$$\eta(\omega,\omega_1,\omega_2) = \chi(\omega,\omega_1,\omega_2)\eta_1(\omega,\omega_1,\omega_2) \tag{6}$$

where η_1 is the single-span kernel, which accounts for the local NLI and is defined as

$$\eta_1 \triangleq \int_0^L e^{-\alpha\zeta}e^{j\Delta\beta\zeta}\mathrm{d}\zeta = \frac{1-e^{-\alpha L}e^{j\Delta\beta L}}{\alpha - j\Delta\beta}, \tag{7}$$

and χ is the following *phased-array* term [20]:

$$\chi \triangleq \sum_{k=1}^{N} e^{j\Delta\beta(k-1)L} = \frac{1-e^{jN\Delta\beta L}}{1-e^{j\Delta\beta L}}, \tag{8}$$

which accounts for the NLI accumulation span-by-span for identical spans [3].

B. Presence of SRS and DGE at every span

In ultra-wideband transmissions, the interplay between SRS and Kerr effect cannot be neglected. The inclusion of SRS in the NLI model calls for a frequency-dependent power profile, due to the nature of the Raman scattering process. An analytical expression of the normalized power profile in the presence of SRS was derived in [12] under the triangular approximation of the Raman gain [11] and the assumption of a frequency-independent fiber attenuation coefficient.

With ideal DGEs and amplifiers after each span, both the SRS gain and the fiber loss are perfectly recovered at the span end. Hence, the normalized power profile becomes

$$\rho(\zeta,\omega) = \Upsilon(L_{\mathrm{eff}}(\zeta))e^{-\alpha\zeta}e^{-P_{\mathrm{t}}C_{\mathrm{r}}L_{\mathrm{eff}}(\zeta)\omega} \tag{9}$$

where: C_{r} is the slope of the linear approximation of the Raman gain, P_{t} is the WDM signal power, and the effective length is defined as $L_{\mathrm{eff}}(\zeta) = \frac{1-e^{-\alpha\zeta}}{\alpha}$.

The factor Υ in Eq. (9) is defined as [12]

$$\Upsilon(L_{\mathrm{eff}}(\zeta)) \triangleq \frac{P_{\mathrm{t}}}{\int_{-\infty}^{\infty} G_{\mathrm{TX}}(\nu)e^{-P_{\mathrm{t}}C_{\mathrm{r}}L_{\mathrm{eff}}(\zeta)\nu}\frac{\mathrm{d}\nu}{2\pi}} \tag{10}$$

where G_{TX} is the power spectral density (PSD) of the transmitted WDM signal. The normalization term Υ ensures that

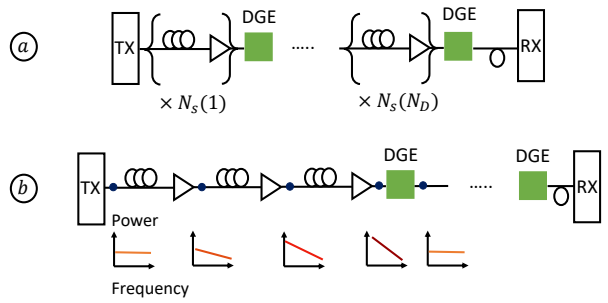

Fig. 1. Sketch of: a) generic link stucture with N_{D} sections having a variable number of spans $N_s(d)$ each, and b) WDM PSD tilt evolution due to accumulated SRS in a link section with $N_s = 3$ spans.

the total power decreases exponentially along the fiber length, namely $P_{\mathrm{t}}(z) = P_{\mathrm{t}}(0)e^{-\alpha z}$. Similarly to the previous section, the normalized power profile is span-independent.

With an ideal DGE after each span the kernel can still be expressed as the product of two terms

$$\eta(\omega,\omega_1,\omega_2) = \chi(\omega,\omega_1,\omega_2)\eta_1^{\mathrm{R}}(\omega,\omega_1,\omega_2) \tag{11}$$

where χ is the phased-array term defined in Eq. (8), while η_1^{R} is a generalization of the single-span η_1 to the case with SRS, equal to [10]

$$\eta_1^{\mathrm{R}} = \int_0^L \Upsilon(L_{\mathrm{eff}}(\zeta))e^{-\alpha\zeta}e^{-P_{\mathrm{t}}C_{\mathrm{r}}L_{\mathrm{eff}}(\zeta)(\omega+\omega_1+\omega_2)}e^{j\Delta\beta\zeta}\mathrm{d}\zeta \tag{12}$$

$$\approx \Big(1-S\Big)\eta_1 + \frac{1-e^{2\alpha L}e^{j\Delta\beta L}}{2\alpha - j\Delta\beta}S \tag{13}$$

where $S \triangleq \frac{P_{\mathrm{t}}C_{\mathrm{r}}(\omega+\omega_1+\omega_2)}{\alpha}$, and η_1 is given in Eq. (7). The last approximation has been derived in [14] and is justified when the power is uniformly distributed across the WDM bandwidth and SRS is weak. Note that in this framework $\Upsilon \approx 1$.

The triangular approximation of the Raman gain holds for bandwidths not exceeding $\approx$ 15 THz [11]. For larger bandwidths, not only the triangular approximation of the Raman gain fails, but also the frequency dependence of the attenuation must be included [21].

C. Presence of accumulated SRS

In this scenario, the Raman gain-tilt is not recovered at every span by a DGE. As a result, the SRS accumulates between two DGEs undermining the assumptions that lead to Eq. (13). Moreover, the absence of gain equalization at the end of each span allows other residual gains/losses to accumulate from span to span. Fig. 1(a) sketches an example. The link is composed of N_{D} link sections, identified by the presence of a DGE at the end of each section. In the most general case, the sections can have a different number of spans N_{s} each. To highlight the effects of the SRS accumulation across the spans, Fig. 1(b) sketches an example of the signal PSD evolution in the first section of a link with $N_{\mathrm{s}} = 3$ spans.

Similar scenarios were considered in [8], where the accumulation of Raman scattering was included by numerically solving the power evolution. Here we propose an analytical expression of the power profile.

Let us focus on a given link section. The PSD of the signal at the input of the kth span, $k \in (1,\ldots,N_s)$, should account for the accumulated SRS and any extra gain/loss $\Lambda(\omega)$:

$$G_k(\omega) = G_{\mathrm{TX}}(\omega)e^{-P_{\mathrm{t}}C_{\mathrm{r}}((k-1)L_{\mathrm{eff}}(L))\omega}\Lambda(\omega)^{(k-1)}. \tag{14}$$

Please note that $\Lambda(\omega)$ reduces to 1 when a DGE is placed at the end of each span. The normalization factor should change accordingly:

$$\Upsilon_k(L_{\mathrm{eff}}(\zeta)) \triangleq \frac{P_{\mathrm{t}}}{\int_{-\infty}^{\infty}G_k(\nu)e^{-P_{\mathrm{t}}C_{\mathrm{r}}L_{\mathrm{eff}}(\zeta)\nu}\frac{\mathrm{d}\nu}{2\pi}} \tag{15}$$

where ζ is the local coordinate within the kth span. In this framework, the normalized power profile between two neighboring DGEs can be written as

$$\rho_k(\zeta,\omega) = \Upsilon_k(L_{\mathrm{eff}}(\zeta))\Lambda(\omega)^{(k-1)}e^{-\alpha\zeta}\times e^{-P_{\mathrm{t}}C_{\mathrm{r}}(L_{\mathrm{eff}}(\zeta)+(k-1)L_{\mathrm{eff}}(L))\omega}. \tag{16}$$

It is worth noting that Eq. (16) does not hold with a frequency-dependent attenuation $\alpha(\omega)$, since the signal power profile has been derived with a frequency-independent loss [12]. As an approximation, Eq. (16) can be used as well by forcing a constant $\alpha(\omega) \equiv \alpha$ *only* in the attenuation profile at local coordinate ζ, while its full profile $\alpha(\omega)$ can be left in the accumulated gain/loss term $\Lambda(\omega)$. Contrary to the previous cases, the power profile in Eq. (16) is span-dependent.

The substitution of the new power profile Eq. (16) in Eq. (3) yields the link kernel expression

$$\eta = \sum_{d=1}^{N_{\mathrm{D}}} e^{j\Delta\beta(d-1)LN_{\mathrm{s}}(d)} \sum_{k=1}^{N_{\mathrm{s}}(d)} e^{j\Delta\beta(k-1)L}g(\omega,\omega_1,\omega_2)^{\frac{k-1}{2}} \times e^{-P_{\mathrm{t}}C_{\mathrm{r}}(k-1)L_{\mathrm{eff}}(L)(\omega+\omega_1+\omega_2)}\eta_k^{\mathrm{R}}(\omega,\omega_1,\omega_2) \tag{17}$$

where d is the index of the link section between two DGEs, $N_{\mathrm{s}}(d)$ is the number of spans in the dth link section, k is the span index within a section, and the term $g(\omega,\omega_1,\omega_2)$ collecting extra gains/losses is defined as

$$g(\omega,\omega_1,\omega_2) = \frac{\Lambda(\omega+\omega_1)\Lambda(\omega+\omega_2)\Lambda(\omega+\omega_1+\omega_2)}{\Lambda(\omega)}. \tag{18}$$

The single-span kernel generalizes to:

$$\eta_k^{\mathrm{R}} = \int_0^L \Upsilon_k(L_{\mathrm{eff}}(\zeta))e^{-\alpha\zeta}e^{-P_{\mathrm{t}}C_{\mathrm{r}}L_{\mathrm{eff}}(\zeta)(\omega+\omega_1+\omega_2)}e^{j\Delta\beta\zeta}\mathrm{d}\zeta \tag{19}$$

with the main difference with Eq. (12) that the normalization factor depends on the span index within the link section, as per Eq. (15).

Since the exponential SRS in Υ includes also the accumulated gain, the weak SRS assumption used in [14] yielding $\Upsilon \approx 1$ may not be justified in this more general scenario with sparse DGEs. As a direct consequence, the z-integral in Eq. (3) cannot be expressed in closed-form and requires to be evaluated through numerical integration. For this reason, in this work we refer to this model as the *integral model*.

Contrary to Sections II-A and II-B, it is not possible to simply identify a phased-array term accounting for the

accumulated effects between spans, since the spans are not all identical due to the absence of a DGE at some spans.

The outer summation over d in Eq. (17) accounts for the dispersion accumulated in the previous link sections. Note that there is no accumulated SRS from previous link sections since each section ends with an ideal DGE. The inner summation over k, on the other hand, accounts for both dispersion and SRS accumulated within the section.

We note that the proposed model can be easily generalized to account for a non-uniform power allocation. For instance, a power pre-emphasis might be applied to the transmitted signal in order to counteract the SRS effect [8], [9], [17]. We find convenient to investigate a pre-emphasis in the form of an SRS gain with opposite sign, namely

$$P(0,\omega) = P_{\mathrm{TX}}(\omega)\frac{P_{\mathrm{t}} e^{\overline{k} P_{\mathrm{t}} L_{\mathrm{eff}}(L) C_{\mathrm{r}} \omega}}{\int_{-\infty}^{\infty} G_{\mathrm{TX}}(\nu) e^{\overline{k} P_{\mathrm{t}} C_{\mathrm{r}} L_{\mathrm{eff}}(L)\nu} \frac{\mathrm{d}\nu}{2\pi}} \tag{20}$$

where $P_{\mathrm{TX}}(\omega)$ is the signal power at the transmitter before the pre-emphasis. Using this notation, the pre-emphasis is governed by the factor $\overline{k}$ which indicates the amount of SRS that is pre-compensated, expressed in number of spans. As a consequence, the link kernel in Eq. (17) can be applied verbatim after the following substitution in the Raman exponential:

$$(k-1) \xrightarrow[\text{pre-emphasis}]{\text{with}} (k-\overline{k}-1) \tag{21}$$

where $k-\overline{k}$ plays the role of an equivalent span index. Examples of the model generalization to include power pre-emphasis will be showed in Section IV.

To first approximation, a similar idea can be used even for non-ideal DGEs by using a $\overline{k}(d)$. Here, $\overline{k}(d)$ indicates the residual fraction of SRS at the beginning of the dth link section, while $k+\overline{k}(d)$ stands for an equivalent span index.

III. Approximated models

The numerical effort to evaluate the general kernel in Eq. (17) with sparse DGEs is particularly heavy since the integrand function is quickly oscillating, thus requiring many function evaluations for an accurate result. For this reason, in this section we introduce approximations of the z-integral in Eq. (17), with big savings in computational time. For the sake of simplicity and generality, we search for an approximation yielding a link kernel in the same form as the one without SRS accumulation, i.e.,

$$\eta(\omega,\omega_1,\omega_2) \approx \chi^{\mathrm{R}}(\omega,\omega_1,\omega_2)\eta_1^{\mathrm{R}}(\omega,\omega_1,\omega_2) \tag{22}$$

where η_1^{R} is the single-span kernel in Eq. (13) and χ^{R} is an inter-span term. Note that Eq. (22) differs from the model without accumulated SRS only in the term χ^{R}.

A. Simplified model

Removing the dependence of Υ on z yields great numerical savings since the remaining integral can be evaluated in closed-form. This idea was implicit in [14] where Υ was approximated to 1, as a result of a weak-SRS assumption. As commented before, this approximation does no longer hold with sparse DGE positioning, hence it must be properly adapted to the new scenario. Since Υ is a monotonic function of $L_{\mathrm{eff}}(\zeta)$, it can be bounded by $\Upsilon(L_{\mathrm{eff}}(L)) \le \Upsilon(L_{\mathrm{eff}}(\zeta)) \le \Upsilon(0)$. Hence, it seems reasonable to approximate the integral in Eq. (19) by a weighted midpoint numerical quadrature [22]. To further increase the accuracy, we perform such an approximation after making the change of variable $L_{\mathrm{eff}}(\zeta) = y$, namely:

$$\begin{aligned}\eta_k^{\mathrm{R}} &= \int_0^{L_{\mathrm{eff}}(L)} \Upsilon_k(y) e^{-P_{\mathrm{t}} C_{\mathrm{r}} y(\omega+\omega_1+\omega_2)} e^{-j\frac{\Delta\beta}{\alpha}\ln(1-\alpha y)} \mathrm{d}y \\ &\approx \Upsilon_k\Big(\frac{L_{\mathrm{eff}}(L)}{2}\Big)\eta_1^{\mathrm{R}}(\omega,\omega_1,\omega_2)\end{aligned} \tag{23}$$

where the exponential functions have been used as the weighting function. $\eta_1^{\mathrm{R}}(\omega,\omega_1,\omega_2)$ is the single-span kernel without accumulated SRS expressed in a closed-form as in Eq. (13). The midpoint rule has an error scaling with $\mathcal{O}(L_{\mathrm{eff}}(L)^3)$ [22] hence is a good compromise between accuracy and simplicity. As a result of the approximation, we thus propose to approximate the local term $L_{\mathrm{eff}}(\zeta)$ in Eq. (15) with a lumped factor $\frac{1}{2}L_{\mathrm{eff}}(L)$, obtaining the following midpoint normalization factor

$$\Upsilon_k \triangleq \frac{P_{\mathrm{t}}}{\int_{-\infty}^{\infty} G_{\mathrm{TX}}(\nu)\Lambda(\nu)^{(k-1)} e^{-P_{\mathrm{t}} C_{\mathrm{r}}(k-\frac{1}{2}) L_{\mathrm{eff}}(L)\nu} \frac{\mathrm{d}\nu}{2\pi}}. \tag{24}$$

Thanks to this approximation, the link kernel in Eq. (17) can be written as

$$\begin{aligned}\eta = \sum_{d=1}^{N_{\mathrm{D}}} e^{j\Delta\beta(d-1)LN_{\mathrm{s}}(d)} \sum_{k=1}^{N_{\mathrm{s}}(d)} e^{j\Delta\beta(k-1)L} g(\omega,\omega_1,\omega_2)^{\frac{k-1}{2}} \\ \times e^{-P_{\mathrm{t}} C_{\mathrm{r}}(k-1) L_{\mathrm{eff}}(L)(\omega+\omega_1+\omega_2)} \Upsilon_k \eta_1^{\mathrm{R}}(\omega,\omega_1,\omega_2)\end{aligned} \tag{25}$$

which can now be easily expressed in the compact form of Eq. (22), where we defined

$$\begin{aligned}\chi^{\mathrm{R}} \triangleq \sum_{d=1}^{N_{\mathrm{D}}} e^{j\Delta\beta(d-1)LN_{\mathrm{s}}(d)} \sum_{k=1}^{N_{\mathrm{s}}(d)} e^{j\Delta\beta(k-1)L} g(\omega,\omega_1,\omega_2)^{\frac{k-1}{2}} \\ \times e^{-P_{\mathrm{t}} C_{\mathrm{r}}(k-1) L_{\mathrm{eff}}(L)(\omega+\omega_1+\omega_2)} \Upsilon_k.\end{aligned} \tag{26}$$

We call *simplified model* the NLI model based on the link kernel of Eq. (25) which relies on the approximated normalization factor defined in Eq. (24).

B. GN-term closed-form expressions

In this section, we generalize the closed-form expressions of the SPM and XPM variance, first derived in [14] in a GN-framework with DGE at every span, to the case of accumulated SRS, i.e., sparse DGE positioning along the link.

For the reader's convenience, we report here the single-span variance expressions. The SPM variance for channel i can be written as [14]

$$\begin{aligned}\sigma^2_{\mathrm{SPM},1}(i) \approx \frac{4}{9}\frac{P_i^3}{B_i^2}\frac{\gamma^2\pi}{\phi_i 3\alpha^2} \times \\ \Big[\frac{T_i-\alpha^2}{\alpha}\mathrm{asinh}\Big(\frac{\phi_i B_i^2}{\pi\alpha}\Big) + \frac{4\alpha^2-T_i}{2\alpha}\mathrm{asinh}\Big(\frac{\phi_i B_i^2}{2\pi\alpha}\Big)\Big]\end{aligned} \tag{27}$$

with $\phi_i = \frac{3}{2}\pi^2(\beta_2 + \beta_3\omega_i)$, $T_i = (2\alpha - P_\mathrm{t}C_\mathrm{r}\omega_i)^2$, and $\omega_i \triangleq 2\pi f_i$, with f_i the lowpass carrier frequency of channel i, referred, without loss of generality, to the reference system centered at the WDM central frequency [14]. The XPM contribution of the ℓth interfering channel to channel i is

$$\sigma^2_{\mathrm{XPM},1}(i,\ell) \approx \frac{32}{27}\frac{P_\ell^2 P_i}{B_\ell}\frac{\gamma^2}{\phi_{i,\ell}3\alpha^2}\times \Big[\frac{T_\ell-\alpha^2}{\alpha}\mathrm{atan}\Big(\frac{\phi_{i,\ell}B_i}{\alpha}\Big)+\frac{4\alpha^2-T_\ell}{2\alpha}\mathrm{atan}\Big(\frac{\phi_{i,\ell}B_i}{2\alpha}\Big)\Big] \quad (28)$$

with B_i the bandwidth of channel i, and $\phi_{i,\ell} = \pi(\omega_\ell - \omega_i)[\beta_2 + \frac{1}{2}\beta_3(\omega_\ell+\omega_i)]$. The approximation is reliable if $|\omega_i - \omega_\ell| \gg 2\pi B_i$ [14].

The NLI accumulation of channel i along the link is usually approximated through the simple scaling rules [3]

$$\sigma^2_{\mathrm{SPM},N}(i) = \mathcal{N}_i^{1+\varepsilon}\,\sigma^2_{\mathrm{SPM},1}(i) \quad (29)$$

$$\sigma^2_{\mathrm{XPM},N}(i) = \sum_{\ell\neq i}\mathcal{N}_\ell\,\sigma^2_{\mathrm{XPM},1}(i,\ell) \quad (30)$$

where the scaling factor is defined as $\mathcal{N}_\ell \triangleq |\chi(0,0,\omega_\ell)|^2_{\mathrm{inc}}$ and the subscript inc indicates that only the incoherent contribution is taken into account, i.e., correlations between different spans are neglected. The coherent NLI accumulation along spans has been included though the factor ε, which plays the role of a coherence correction [3], [23], [24] whose expression in absence of SRS can be found in [3]. As in [14], the coherence factor is included only in the SPM accumulation in Eq. (29).

Note that the scaling rules in Eq. (29) and (30) require the accumulated effects to be factored out by the term χ. Unfortunately, the NLI model in the presence of accumulated SRS proposed in Section II-C cannot be cast in this form. On the other hand, the simplified model presented in this section can be expressed in such a form as in Eq. (22). Therefore, the simplified model opens the path to closed-form expressions in the presence of accumulated SRS.

For a single-span, η_1^{R} in the simplified model coincides with the closed-form expression of the single-span z-integral derived in [14], therefore the single-span SPM and XPM variance expressions in Eq. (27) and Eq. (28) still hold in this framework. On the other hand, in a multi-span link the term $\mathcal{N}$ must be modified to account for sparse DGE positioning along the distance, as summarized in Tab. I. Note that this term simply reduces to the number of spans N when there is no accumulated SRS, including the absence of local SRS, as in [3] and [14]. Please note that although the summations in the novel simplified model cannot be expressed in closed-form, they can be quickly evaluated numerically. Moreover, the outer summation simply reduces to N_D if all the link sections are equal.

As observed for the integral model, both the simplified model and the closed-form expressions can be generalized to include SRS pre-compensation through an equivalent span index as in Eq. (21).

TABLE I
SCALING FACTOR $\mathcal{N}_\ell$ FOR NLI ACCUMULATION WITH SPANS.

Case	Scaling factor $\mathcal{N}_\ell$
$N_\mathrm{s}=1$	N
$N_\mathrm{s}>1$ simplified model	$\sum_{d=1}^{N_\mathrm{D}}\sum_{k=1}^{N_\mathrm{s}(d)}\Upsilon_k^2\Lambda(\omega_\ell)^{2(k-1)}e^{-2P_\mathrm{t}C_\mathrm{r}L_\mathrm{eff}(L)\omega_\ell(k-1)}$
$N_\mathrm{s}>1$ integral model	not available

After SRS gain equalization on the desired signal at the receiver, the SNR of a generic WDM channel centered at frequency ν can be written as

$$\mathrm{SNR} = \frac{P}{\sigma^2_{\mathrm{NLI}}+\sigma^2_{\mathrm{ASE}}} \quad (31)$$

where σ^2_{NLI} is the channel NLI variance and σ^2_{ASE} is the ASE noise variance. For a system with all identical devices and fibers, such variances take simple expressions. In the absence of SRS the NLI variance scales with P^3 [25], [26], while the ASE variance at the end of a link composed of N identical amplifiers with frequency-flat gain G and noise figure F is equal to $\sigma^2_{\mathrm{ASE}} = N \times h\nu FGB$, where h is the Planck's constant, and B is receiver noise equivalent bandwidth.

In the presence of SRS, σ^2_{NLI} does not scale anymore with P^3 since the fiber kernel depends on the total power, while the ASE variance can be generalized as follows:

$$\sigma^2_{\mathrm{ASE}} = h\nu FGB\sum_{d=1}^{N_\mathrm{D}}\sum_{k=1}^{N_\mathrm{s}(d)}\frac{\rho_{N_s(d)-k}}{\rho_{N_s(d)}} \quad (32)$$

where ρ is evaluated at the span end and at frequency ν as per Eq. (16). Namely, the ASE noise introduced by the kth amplifier in the dth link section is affected by SRS in each of the subsequent $N_s(d)-k$ spans (hence the factor $\rho_{N_s(d)-k}$) and by the DGE frequency response at the end of the link section (factor $\rho_{N_\mathrm{s}(d)}$). Since the main focus of this work is the impact of accumulated SRS on the NLI, in the following we will concentrate mainly on the NLI variance.

IV. NUMERICAL RESULTS

We implemented both the integral and the approximated model by adopting the link kernel expressions in Eq. (17) and Eq. (25), respectively, in the EGN model [2], [16]. Throughout this section, we will refer to the respective EGN models with the labels integral DGE-SRS-EGN and simplified DGE-SRS-EGN model. In particular, in both models, the frequency integrals involved in the variance computation are performed by means of Monte Carlo integration [2], [27], and all the nonlinear effects (SPM, XPM, FWM, XCI and MCI according to the nomenclature in [2]) are included. The z-integration of the integral model is implemented by means of Filon's quadrature method [28] for oscillating integrands. On the other hand, the simplified DGE-SRS-EGN model relied on

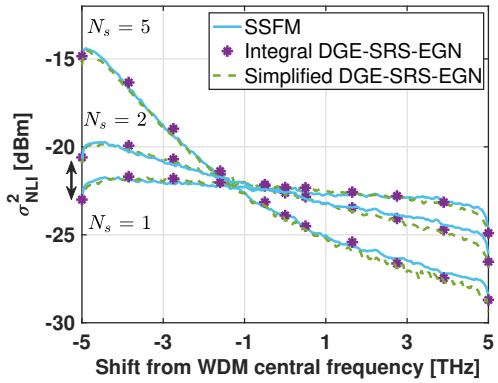

Fig. 2. NLI variance $\sigma^2_{\rm NLI}$ versus frequency shift. PDM-64QAM, 201 channels, 10 × 100 km with DGE period $N_{\rm s} = 1, 2$ or 5 spans. Solid line: SSFM simulations. Markers: Integral DGE-SRS-EGN. Dashed line: simplified DGE-SRS-EGN model.

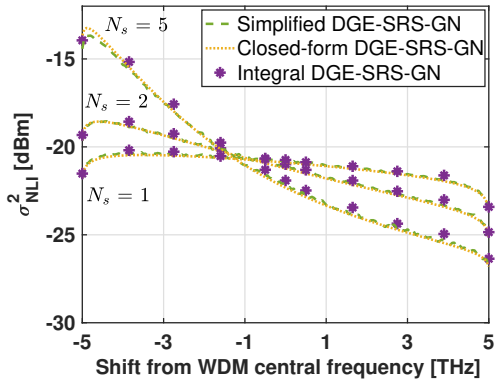

Fig. 4. NLI variance $\sigma^2_{\rm NLI}$ versus frequency shift. Gaussian distributed symbols, 201 channels, 10 × 100 km with DGE period $N_{\rm s} = 1, 2$ or 5 spans. Markers: Integral DGE-SRS-GN. Dashed line: simplified DGE-SRS-GN. Dotted: extended-closed forms.

the closed-form expression of the single-span kernel, as well as the GN-term closed-form expressions.

The links under test were dispersion-uncompensated, composed of single-mode fibers (SMFs) and based on ideal end-span lumped amplification with frequency-flat gain. The SRS gain on the signal was recovered by ideal DGEs, with variable number and position along the link. The SMFs had length $L = 100$ km, frequency-flat attenuation $\alpha = 0.2$ dB/km, dispersion $D = 17$ ps/(nm·km), dispersion slope $S = 0.057$ ps/(nm^2·km), and nonlinear coefficient $\gamma = 1.26$ 1/(W·km). The slope of the triangular approximation of the Raman gain of the fiber was $C_{\rm r} = 0.028/(2\pi)$ (THz·rad·km·W)$^{-1}$.

While the EGN model relies on the triangular approximation of the Raman gain, in the SSFM simulations we used a polynomial interpolation of the experimental gain [2], accounting for both the real and the imaginary part of the Raman spectrum.

The WDM was a comb of polarization division multiplexed signals with channel spacing $\Delta f = 50$ GHz. Each channel was shaped with root-raised cosine pulses of 0.01 roll-off, and modulated at the symbol rate 49 Gbaud. The number of symbols was 67550, and the SSFM symmetric-step was updated according to the constant local error criterion with a maximum tolerable FWM phase matching $\Delta\phi_{\rm FWM}$= 10 rad [29]. At the receiver, ideal chromatic dispersion compensation was followed by a matched filter detection and a least-squares equalizer with 1 tap that recovered the average polarization and phase mismatch. The NLI variance in the SSFM simulations was estimated as the variance of the difference between the received and the transmitted sequence of symbols, in the absence of ASE noise.

In a first test we investigated 64-quadrature amplitude modulation (64QAM) signals with a 0 dBm transmitted power per channel, over a WDM bandwidth of 10 THz. Such a channel power is close to the power maximizing the SNR of the central channel in the absence of SRS and with noise figure $F = 5$ dB. Figure 2 shows the NLI variance versus the frequency shift after 10 spans with DGE placed every 1, 2, or 5 spans. We used solid lines for SSFM results, markers for the integral DGE-SRS-EGN model, and dashed lines for the simplified DGE-SRS-EGN model. It can be seen that both the integral and the simplified EGN models proposed in this work correctly estimate the impact of accumulated SRS on the NLI. Both models exhibit an average error across the WDM bandwidth smaller than 0.3 dB for each DGE placement configuration, with the largest value concentrated at the bandwidth edges. In particular, we verified with an extra-simulation here not reported that the error of the integral DGE-SRS-EGN model is mainly related to the underlying triangular approximation of the Raman gain.

Most important, it can be seen that the NLI tilt is emphasized by the accumulation of SRS between DGEs, yielding curves with $N_{\rm s} > 1$ far apart from the benchmark $N_{\rm s} = 1$ case usually analyzed in the literature. For instance, even with a DGE every two spans, i.e., $N_{\rm s} = 2$, the gap with the curve having a DGE at every span, highlighted by the double arrow in the figure, is up to ≈ 2 dB.

Then, we verified the accuracy of the proposed models for a 16QAM modulation, for the same set-up of Fig. 2. Figure 3 shows a good agreement between theory and SSFM simulations, with similar accuracy as that of the 64QAM case.

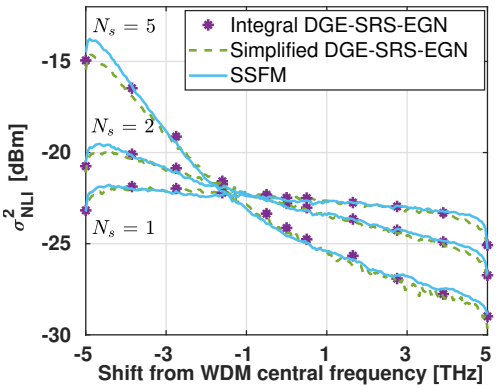

Fig. 3. NLI variance $\sigma^2_{\rm NLI}$ versus frequency shift. PDM-16QAM, 201 channels, 10 × 100 km with DGE period $N_{\rm s} = 1, 2$ or 5 spans. Solid line: SSFM simulations. Markers: Integral DGE-SRS-EGN. Dashed line: simplified DGE-SRS-EGN model.

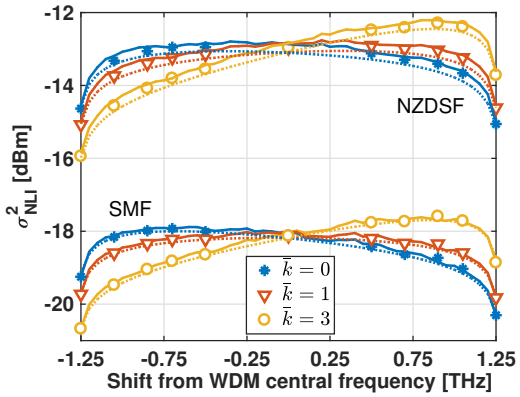

Fig. 5. NLI variance $\sigma^2_{\rm NLI}$ versus frequency shift. Gaussian distributed symbols, 51 channels, 3 $\times$ 100 km of SMFs or NZDSFs, without inline DGEs. Variable pre-emphasis factor $\bar{k}$, see Eq. (20). Solid: SSFM. Markers: Integral DGE-SRS-GN model. Dotted: extended-closed forms by using Eq. (20).

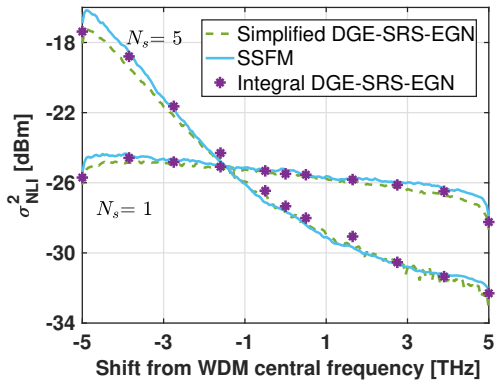

Fig. 6. NLI variance $\sigma^2_{\rm NLI}$ versus frequency shift. PDM-64QAM, 201 channels, 5 $\times$ 100 km of ULL fiber with DGE period $N_{\rm s} = 1, 5$ spans. Solid line: SSFM simulations with $\alpha(\omega)$. Dashed line: simplified DGE-SRS-EGN. Makers: integral DGE-SRS-EGN.

It is worth noting that simulating the transmission of 10 THz over 1000 km via SSFM had a nearly prohibitive cost in terms of computational time, requiring at least 21 days for each curve in Fig. 2 and 3 using graphical process units (GPUs).

As an example of the complexity reduction enabled by the simplified model, we report the computational times required to compute the NLI variance with the two models. Using a server-grade architecture, the integral model required $\approx$ 50 min/channel to compute the NLI variance of Fig. 2. The simplified model required less than 1 min/channel by using the same number of Monte Carlo samples for frequency integration.

The computational time can be further reduced by replacing the Monte Carlo integrations in the frequency domain with the closed-form expressions. Although such expressions can be computed in a few seconds, it is worth noting that they i) account only for SPM and XPM, ii) postulate a scaling of SPM with the coherence factor ε, iii) use the same ε as the case without SRS, and iv) assume Gaussian distributed symbols. We thus investigated the reliability of such expressions with Gaussian distributed symbols, while all the other link and transmission parameters were those of Fig. 2. The corresponding NLI variance, as well as its estimation by the integral and the simplified model, are reported in Fig. 4. The dotted lines represent the closed-form results, the solid lines indicate the simplified Monte Carlo model while the markers represent the $\sigma^2_{\rm NLI}$ obtained with the integral model. The figure shows that the average gap between the closed-form and its Monte Carlo counterpart is less than 0.1 dB for all the DGE periods, making the closed-form expression a fast reliable alternative for estimations with Gaussian distributed symbols. The closed-form expression accuracy is expected to decrease when low-dispersion fibers or low symbol rates are taken into account, due to the higher relative contribution of FWM.

A. Signal power pre-emphasis

We checked the validity of the model with signal power pre-emphasis as per Eq. (20). Since SSFM simulations of 10 THz over 1000 km are extremely time consuming, we focused on a faster set-up by reducing the bandwidth and the link length. We thus transmitted 51 channels, with the same frequency spacing and symbol rate as in the previous figures, with channel power $P = 3$ dBm.

To test the impact of the pre-emphasis only, we estimated the NLI variance after 300 km, without intermediate DGEs. We considered both SMFs and non-zero dispersion-shifted fibers (NZDSFs), with dispersion parameter $D = 17$ ps/(nm·km) and $D = 4.5$ ps/(nm·km), respectively. For the sake of comparison, the NZDSF under test differed from the SMF considered so far only in the dispersion coefficient. For both cases, we report the NLI variance in the absence of SRS pre-compensation ($\bar{k} = 0$) and for two pre-emphasis choices $\bar{k}=1, 3$. We recall that, according to Eq. (21), a pre-emphasis factor of $\bar{k}$ yields a frequency-flat signal power after $\bar{k}$ spans.

Figure 5 shows the NLI variance estimated with SSFM simulations, the integral DGE-SRS-EGN model and the closed-form expressions modified according to Eq. (21). It can be seen that the simulations are in good agreement with the theory. In particular, the modified closed-forms exhibit a maximum error of $\approx$ 0.25 dB with SMFs, and an average error across the WDM bandwidth smaller than 0.1 dB. The maximum gap slightly increases to 0.3 dB with NZDSFs, while on average it is 0.2 dB. This can be mainly attributed to the absence of FWM, XCI and MCI terms in the closed-forms, whose relative contribution to the overall NLI increase at lower dispersion.

B. Frequency-dependent attenuation

In this section, we check the validity of Eq. (16) with a frequency-dependent fiber attenuation. To this aim, we included a frequency-dependent attenuation profile in the SSFM simulations. Here we changed the fiber, a Corning ULL, for which an experimental attenuation profile is available in [21] and we approximated such a profile with a quadratic fitting polynomial.

The link was composed of $N = 5$ spans with DGE repetition every 1 and 5 spans. Each amplifier had a frequency-

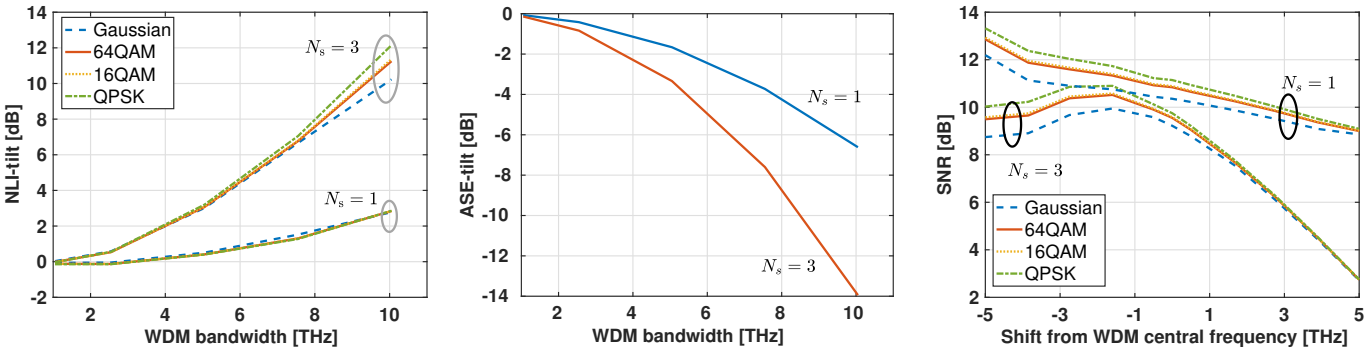

Fig. 7. For a 30×100 km link with DGE repetition every $N_\mathrm{s} = 1$ and $N_\mathrm{s} = 3$ spans: (a) NLI variance tilt in dB (between the two edge WDM channels) for QPSK (dash-dotted), 16QAM (dotted), 64QAM (solid) and Gaussian (dashed) transmissions versus WDM bandwidth; (b) ASE variance tilt in dB versus WDM bandwidth; (c) SNR versus frequency offset from central channel at WDM bandwidth 10 THz.

independent gain restoring the nominal total power. Therefore, a frequency-dependent residual loss accumulated up to a DGE.

Figure 6 shows the NLI variance estimated with SSFM simulations, the integral and the simplified DGE-SRS-EGN model with *local* fiber attenuation coefficient in Eq. (16) equal to $\alpha = 0.162$ dB/km. The average error across the WDM bandwidth between simulations and theory is less than 0.3 dB for $N_\mathrm{s} = 1$, meaning that neglecting the local effects of the frequency-dependent fiber attenuation as in Eq. (16) has a minor impact on the NLI, consistently with the discussion in [10]. When the DGE period is increased to $N_\mathrm{s} = 5$ spans, the average error is ≈ 0.3 dB.

In particular, we note that the impact of a sparse DGE positioning on the NLI variance is barely affected by the frequency-dependent fiber attenuation. Figure 6 shows a maximum gap of ≈ 8 dB between the curves with $N_\mathrm{s} = 1$ and 5 spans, which is comparable to the gap estimated with a frequency-flat fiber attenuation.

C. Modulation format

We next investigate the joint impact of the modulation format and the accumulated SRS on the NLI variance using the simplified model. We considered the transmission of a $B_\mathrm{t} = 0.05 \times N_\mathrm{ch}$ THz WDM comb with variable bandwidth $B_\mathrm{t} = (1, 2.5, 5, 7.5, 10)$ THz, associated to $N_\mathrm{ch} = (21, 51, 101, 151, 201)$ channels, respectively. The channel power was fixed to 1 dBm.

We considered different modulation formats: Gaussian, 64QAM, 16QAM, and quadrature phase-shift keying (QPSK). The link under test was composed of 30 spans of SMFs with DGE placed every 1 or 3 spans. For each scenario, we measured the tilt of the variance as the difference between the value in dB over the first and the last WDM channel in frequency.

Figure 7(a) shows the SRS-induced NLI variance tilt as a function of the WDM bandwidth. It can be seen that, with a DGE after each span, the NLI-tilt is almost independent of the modulation format. This observation is consistent with the results reported in the literature [15], [16]. On the other hand, when the DGE period is increased to 3 spans, the tilt increases significantly as the bandwidth increases. For the extreme case of $B_\mathrm{t} = 10$ THz, we estimated ≈ 2 dB of difference between the tilt of PDM-QPSK and PDM-Gaussian transmission.

For the sake of completeness, we report in Figure 7(b) the ASE variance tilt for the same link. Note that the ASE variance undergoes an SRS-induced tilt with an opposite sign compared to the NLI variance, yet not identical in absolute value.

We then estimated the received SNR by using frequency-flat noisy amplifiers with noise figure 5 dB. Figure 7(c) shows the SNR versus the frequency offset from the central channel at $B_\mathrm{t} = 10$ THz, with DGE placed every 1 and 3 spans. It can be seen that the SRS-induced tilt on the SNR with $N_\mathrm{s} = 1$ does depend on the modulation format although the NLI-tilt is almost format-independent. Therefore, the error introduced in the SNR estimation by neglecting the modulation format is frequency-dependent.

Figure 7(c) also shows that the SNR non-flatness in frequency is enhanced by the presence of accumulated SRS. In particular, the SNR deviation across the WDM bandwidth increases by ≈ 4 dB when the number of spans between the equalizers increases from 1 to 3.

It is worth noting that such tilts on the ASE and NLI have different implications on the system design. For instance, a

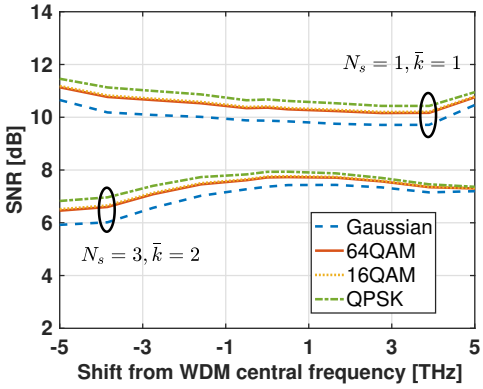

Fig. 8. SNR versus frequency shift. Same setup of Fig. 7(c) with power pre-emphasis factor $\bar{k}$ in Eq. (20) optimized to reduce the SNR variations in frequency.

1 dB variation in the NLI variance, ASE variance, or SNR, corresponds approximately to a deviation of $1/3$, $2/3$, and 1 dB, respectively, in the system reach [30, p. 324]. The same scaling laws apply even for the errors introduced by the models.

In order to counteract this undesired imbalance in the SNR and achieve similar performance on all the WDM channels, a power pre-emphasis can be applied at the transmitter side [8], [9], [17]. Figure 8 shows the SNR estimation versus frequency, for the same setup of Fig. 7(c), with signal power pre-emphasis as per Eq. (20). The pre-emphasis factor $\bar{k}$ was optimized to minimize the maximum SNR difference between two arbitrary channels at fixed total power. Namely, the pre-emphasis factor was $\bar{k} = 1$ for $N_\mathrm{s} = 1$ and $\bar{k} = 2$ for $N_\mathrm{s} = 3$. Please note that a fast optimization of the pre-emphasis factor is possible thanks to the proposed simplified DGE-SRS-EGN model.

In the absence of signal power pre-emphasis, in Fig. 7(c) we measured up to 8 dB of SNR imbalance for the case having $N_\mathrm{s} = 3$, and up to 4 dB with $N_\mathrm{s} = 1$. On the other hand, Fig. 8 shows that the maximum SNR deviation in frequency is $\approx$ 1.5 dB for Gaussian distributed symbols and $\approx$ 1.1 dB for QPSK, with optimized pre-emphasis factor $\bar{k}$.

Although the pre-emphasis through $\bar{k}$ is sub-optimal and counteracts only the SRS tilt, the simplicity of the generalized simplified model and its approximated closed-form formulas is remarkable. Such models can be used for fast predictions of system performance closer to reality than existing models unaware of pre-emphasis. More accurate predictions with arbitrary pre-emphasis can be obtained by using the integral model.

D. Self- and Cross-channel nonlinear effects

Finally, we investigate the accuracy of the simplified DGE-SRS-EGN model on the estimation of SPM and XPM, using the integral DGE-SRS-EGN model as a benchmark. We perform the exploration at variable symbol rates, thus extending the main findings of [31] to SRS.To this aim, we considered the transmission of a 16QAM WDM signal having $B_\mathrm{t} = 10$ THz and $N_\mathrm{ch} = (1601, 801, 401, 201, 101)$ channels with symbol rate $R = (6.125, 12.25, 24.5, 49, 98)$ Gbaud. The relative channel spacing $\Delta f/R$ was fixed to 1.02 and the total WDM power was $P_\mathrm{t} = 23$ dBm. The link under test was composed of 20 spans of SMFs with DGE placed every 4 spans.

The model predictions are depicted in Fig. 9. Figure 9 (a) and (b) show the variance of the first and last WDM channel in frequency, respectively, normalized to the cube of the channel power. FWM is not reported since its variance was estimated to be 6 dB smaller than XPM at 6 Gbaud, with an increasing gap for increasing R. In both figures, it can be seen that the difference between the simplified (dashed) and the integral model (markers) is negligible over the entire symbol rate axis for both nonlinear effects.

In the same figure we also show with dotted lines the same curves in the absence of SRS. The figure shows that the presence of SRS changes the balance between the nonlinear effects in a frequency-dependent manner. For instance, the

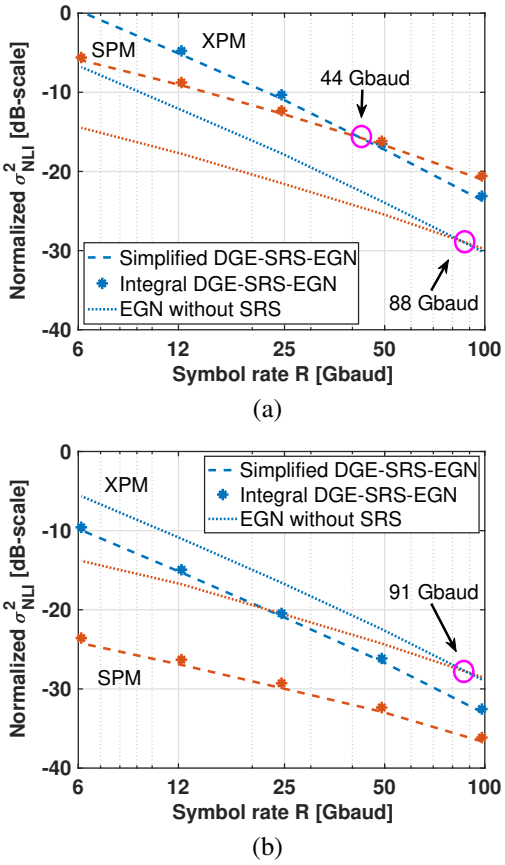

Fig. 9. NLI variance σ^2_{NLI} of SPM and XPM, normalized to the cube of the channel power, versus the symbol rate, estimated for the (a) first, and (b) last WDM channel. PDM-16QAM, $B_\mathrm{t} = 10$ THz, $P_\mathrm{t} = 23$ dBm, 20×100 km of SMFs with DGE period $N_\mathrm{s} = 4$ spans.

SRS-unaware model predicts that the crossing point between SPM and XPM on the first WDM channel occurs at $R = 88$ Gbaud. SRS moves such a point to 44 Gbaud by inflating more SPM than XPM.

An opposite behavior occurs for the last WDM channel, as shown in Fig. 9(b). In the absence of SRS the crossing point is $R = 91$ Gbaud, slightly different from 9(a) because of third-order dispersion. On the contrary, when SRS is taken into account, XPM remains the main nonlinear impairment, being the crossing point with SPM at $R = 510$ Gbaud.

V. Conclusions

We showed that the accumulation of the SRS along the link due to sparse DGE positioning has serious implications on the received NLI variance. We extended the EGN model to account for accumulated SRS by modifying the link kernel. The model is based on a signal power profile expression which accounts for generic DGEs placement along the optical link. However, the new link kernel integral cannot be approximated using known simple closed-form expressions and thus results in undesired additional computational complexity. To reduce the computation time of the NLI variance, we proposed an approximated model for the link kernel. We also proposed a simple generalization of known closed-form expressions [14] to preserve their accuracy in the presence of accumulated SRS.

We validated the extended EGN model against 10 THz SSFM simulations, observing an average gap within 0.3 dB in the considered cases. The closed-form expressions were also cross-validated against their integral counter-part, exhibiting an average error below 0.1 dB. The novel expressions, beside accounting for sparse DGE positioning, can also account for signal power pre-emphasis.

We conclude that the presence of accumulated SRS in the link due to sparse DGE placement cannot be neglected. Its inclusion in the EGN model significantly increases its complexity, which can be substantially reduced by the proposed simplified model. The simplicity of the model can be leveraged for fast optimization of wide-band systems design both in terms of DGE placement along the link and signal power pre-emphasis to counteract the SRS effect.

VI. Acknowledgment

The authors would like to thank Jean-Christophe Antona for valuable comments and suggestions. This research benefits from the high performance computing facility of the University of Parma, Italy.

References

[1] M. Cantono, R. Schmogrow, M. Newland, V. Vusirikala, and T. Hofmeister, "Opportunities and Challenges of C+L Transmission Systems," *J. Lightw. Technol.,* vol. 38, no. 5, pp. 1050-1060, Mar. 2020.

[2] P. Serena, C. Lasagni, S. Musetti and A. Bononi, "On Numerical Simulations of Ultra-Wideband Long-Haul Optical Communication Systems," *J. Lightw. Technol*., vol. 38, no. 5, pp. 1019-1031, Mar. 2020.

[3] P. Poggiolini, "The GN model of non-linear propagation in uncompensated coherent optical systems," *J. Lightw. Technol.,* vol. 30, no. 24, pp. 3857-3879, Dec. 2012.

[4] A. Carena, G. Bosco, V. Curri, Y. Jiang, P. Poggiolini, and F. Forghieri, "EGN model of non-linear fiber propagation," *Opt. Express,* vol. 22, no. 13, pp. 16335-16362, Jun. 2014.

[5] P. Serena and A. Bononi, "A Time-Domain Extended Gaussian Noise Model," *J. Lightw. Technol.,* vol. 33, no. 7, pp. 1459-1472, Apr. 2015.

[6] R. Dar, M. Feder, A. Mecozzi, and M. Shtaif, "Properties of nonlinear noise in long, dispersion-uncompensated fiber links," *Opt. Express,* vol. 21, no. 22, pp. 25685-25699, Nov. 2013.

[7] G. P. Agrawal, *Nonlinear Fiber Optics*, 3rd ed. San Diego, CA: Academic Press, 2001.

[8] I. Roberts, J. M. Kahn, J. Harley, and D. W. Boertjes, "Channel Power Optimization of WDM Systems Following Gaussian Noise Nonlinearity Model in the presence of Stimulated Raman Scattering," *J. Lightw. Technol.,* vol. 35, no. 23, pp. 5237-5250, Dec. 2017.

[9] M. Cantono, D. Pilori, A. Ferrari, C. Catanese, J. Thouras, J. Augé, and V. Curri, "On the Interplay of Nonlinear Interference Generation With Stimulated Raman Scattering for QoT Estimation," *J. Lightw. Technol.,* vol. 36, no. 15, pp. 3131–3141, Aug. 2018.

[10] D. Semrau, R. Killey, and P. Bayvel, "The Gaussian Noise Model in the Presence of Inter-Channel Stimulated Raman Scattering," *J. Lightw. Technol.,* vol. 36, no. 14, pp. 3046-3055, Jul. 2018.

[11] A. R. Charplyvy, "Optical power limits in multi-channel wavelength-division-multiplexed systems due to stimulated Raman scattering," *Electron. Lett.,* vol. 20, no. 2, pp. 58-59, Jan. 1984.

[12] M. Zirngibl, "Analytical model of Raman gain effects in massive wavelength division multiplexed transmission systems," *Electron. Lett.,* vol. 34, no. 8, pp. 789-790, Apr. 1998.

[13] P. Poggiolini, "A generalized GN-model closed-form formula," *arXiv*:1810.06545v2, Nov. 2018.

[14] D. Semrau, R. Killey, and P. Bayvel, "A Closed-Form Approximation of the Gaussian Noise Model in the Presence of Inter-Channel Stimulated Raman Scattering ," *J. Lightw. Technol.*, vol. 37, no. 9, pp. 1924-1936, May 2019.

[15] D. Semrau, E. Sillekens, R. Killey, and P. Bayvel, "A Modulation Format Correction Formula for the Gaussian Noise Model in the Presence of Inter-Channel Stimulated Raman Scattering," *J. Lightw. Technol.,* vol. 37, no. 19, pp. 5122-5131, Oct. 2019.

[16] C. Lasagni, P. Serena and A. Bononi, "A Raman-aware enhanced GN-model to estimate the modulation format dependence of the SNR tilt in C+L band," in *Proc. Eur. Conf. Opt. Commun.*, Dublin, Ireland, 2019, paper W.1.D.2.

[17] D. Semrau, E. Sillekens, P. Bayvel and R. Killey, "Modeling and mitigation of fiber nonlinearity in wideband optical signal transmission," *J. Opt. Commun. Netw.,* vol. 12, no. 6, pp. 68–76, Jun. 2020.

[18] C. Lasagni, P. Serena and A. Bononi, "Impact of Sparse Gain Equalization in the Presence of Stimulated Raman Scattering," in *Proc. Eur. Conf. Opt. Commun.*, Brussels, Belgium, 2020, paper We2F-4.

[19] A. Vannucci, P. Serena, and A. Bononi, "The RP Method : A New Tool for the Iterative Solution of the Nonlinear Schrödinger Equation," *J. Lightw. Technol.,* vol. 20, no. 7, pp. 1102-1112, Jul. 2002.

[20] M. Nazarathy, J. Khurgin, R. Weidenfeld, Y. Meiman, P. Cho, R. Noe, I. Shpantzer, and V. Karagodsky, "Phased-array cancellation of nonlinear FWM in coherent OFDM dispersive multi-span links," *Opt. Exp*., vol. 16, no. 20, pp. 15778–15810, Sep. 2008.

[21] D. Semrau, L. Galdino, E. Sillekens, D. Lavery, R.I. Killey and P. Bayvel, "Modulation format dependent, closed-form formula for estimating nonlinear interference in S+C+L band systems," in in *Proc. Eur. Conf. Opt. Commun.*, Dublin, Ireland, 2019, paper W.1.D.1.

[22] A. Quarteroni, R. Sacco, and F. Saleri, *Numerical Mathematics*, 2nd ed. New York, NY, USA: Springer-Verlag, 2007.

[23] F. Vacondio, O. Rival, C. Simonneau, E. Grellier, A. Bononi, L. Lorcy, J.-C. Antona, and S. Bigo, "On nonlinear distortions of highly dispersive optical coherent systems," *Opt. Express,* vol. 20, no. 2, pp. 1022-1032, Jan. 2012.

[24] G. Bosco, R. Cigliutti, A. Nespola, A. Carena, V. Curri, F. Forghieri, Y. Yamamoto, T. Sasaki, Y. Jiang, and P. Poggiolini, "Experimental investigation of nonlinear interference accumulation in uncompensated links," *IEEE Photon. Technol. Lett.,* vol. 24, no. 14, pp. 1230-1232, Jul. 2012.

[25] G. Bosco, A. Carena, R. Cigliutti, V Curri, P. Poggiolini, and F. Forghieri, "Performance prediction for WDM PM-QPSK transmission over uncompensated links", in *Proc. Opt. Fiber Commun.*, Los Angeles, USA, 2011, paper OTh07.

[26] E. Grellier and A. Bononi, "Quality parameter for coherent transmissions with Gaussian-distributed nonlinear noise," *Opt. Express*, vol. 19, no. 13, pp. 12781-12788, Jun. 2011.

[27] R. Dar, M. Feder, A. Mecozzi, and M. Shtaif, "Accumulation of nonlinear interference noise in multi-span fiber-optic systems," *Opt. Express,* vol. 22, no. 12, pp. 14199-14211, Jun. 2014.

[28] M. Abramowitz, I.A. Stegun, *Handbook of Mathematical Functions with Formulas, Graphs, and Mathematical Tables*, Dover Publications, Inc., 1974

[29] S. Musetti, P. Serena, and A. Bononi, "On the Accuracy of Split-Step Fourier Simulations for Wideband Nonlinear Optical Communications," *J. Lightw. Technol.,* vol. 38, no. 23, pp. 5669-5677, Dec. 2018.

[30] A. Bononi, R. Dar, M. Secondini, P. Serena, and P. Poggiolini, "Fiber Nonlinearity and Optical System Performance," in Springer *Handbook of Optical Networks*, B. Mukherjee, I. Tomkos, M. Tornatore, P. Winzer, and Y. Zhao, Eds. Cham: Springer International Publishing, 2020, pp. 287–351.

[31] P. Poggiolini, A. Nespola, Y. Jiang, G. Bosco, A. Carena, L. Bertignono, S. M. Bilal, S. Abrate, and F. Forghieri, "Analytical and Experimental Results on System Maximum Reach Increase Through Symbol Rate Optimization,"*J. Lightw. Technol.,* vol. 34, no. 8, pp. 1872-1885, Apr. 2016.